Novel Spectrally Efficient UWB Pulses Using Zinc and Frequency-Domain Walsh Basis Functions

Praveen Chaurasiya, Ashkan Ashrafi, and Santosh Nagaraj

In this paper, two sets of spectrally efficient ultra-wideband (UWB) pulses using zinc and frequency-domain Walsh basis functions are proposed. These signals comply with the Federal Communications Commission (FCC) regulations for UWB indoor communications within the stipulated bandwidth of 3.1 GHz to 10.6 GHz. They also demonstrate high energy spectral efficiency by conforming more closely to the FCC mask than other UWB signals described in the literature. The performance of these pulses under various modulation techniques is discussed in this paper, and the proposed pulses are compared with Gaussian monocycles in terms of spectral efficiency, autocorrelation, crosscorrelation, and bit error rate performance.

Keywords: Ultra-wideband communications, orthogonal pulse design, zinc basis functions, Walsh functions, frequency-domain Walsh basis functions.

Manuscript received May 23, 2012; revised Sept. 7, 2012; accepted Oct. 9, 2012.

Praveen Chaurasiya (phone: +1 858 655 1175, pchauras@qualcomm.com) is with the QCT, Qualcomm Inc., San Diego, CA, USA.

Ashkan Ashrafi (corresponding author, ashrafi@mail.sdsu.edu) and Santosh Nagaraj (snagaraj@mail.sdsu.edu) are with the Department of Electrical and Computer Engineering, San Diego State University, San Diego, CA, USA.

http://dx.doi.org/10.4218/etrij.13.0112.0315

I. Introduction

The history of ultra-wideband (UWB) communication can be traced back to the first experiments with wireless transmission. In the late 1800s, J.C. Bose and G. Marconi were working on 60-GHz communication capabilities. In their initial experiments for transmitting radio waves, they used wide bandwidth signals generated by spark gap transmitters [1]. Their initial experiments laid a solid foundation for further research in UWB communication systems. The foundation for modern UWB technology was laid in the sixties when it was developed as a carrier-less transmission technique. In February 2002, the United States Federal Communications Commission (FCC) permitted the use of the 3.1-GHz to 10.6-GHz band for UWB communication devices on an unlicensed basis [2]. This regulation has spurred a considerable amount of research in the design of UWB-related techniques. The UWB communication affords a carrier-free, high data rate, extremely high bandwidth environment with applications in both consumer and military fields. Some of the features of the UWB communication systems are high data rate capability (100 Mbps at 10 m), low equipment complexity and hence low cost, excellent multipath immunity, and the ability to provide multiuser communication capabilities [3]. The FCC introduced a spectral mask for indoor communications, stipulating an allowed frequency range (3.1 GHz to 10.6 GHz) with a contiguous bandwidth of 7.5 GHz and a maximum power spectral density of –41.3 dBm/MHz within this range [2]. These strict guidelines ensure noninterference with existing services in the allocated spectrum. Following the FCC regulation, UWB techniques have been investigated as an attractive solution for short and medium range wireless communication applications.

The unlicensed use of the available wide spectrum by UWB

devices necessitates the development of judicious signaling methods that ensure minimal interference with coexisting narrowband systems. From [4], we use a simplified version of the FCC mask, as described below.

$$P_{\text{mask}}(\omega)=\begin{cases}-40\ \text{dBm}, & 0\le \omega/2\pi \le 3.1\ \text{GHz},\\ 0\ \text{dBm}, & 3.1\ \text{GHz}\le \omega/2\pi \le 10.6\ \text{GHz},\\ -15\ \text{dBm}, & \omega/2\pi \ge 10.6\ \text{GHz}.\end{cases} \quad (1)$$

This mask is tighter than the normalized FCC mask (indoor applications); consequently, all the constraints defined by the FCC regulations are satisfied by (1).

Spectral efficiency (in the frequency domain) and pulse localization (in the time domain) are critical for high data rate, pulsed-UWB communication systems. Compared to narrowband systems, a UWB transmitter transmits a train of extremely short-duration pulses at relatively long time intervals, resulting in a very low power spectral density (close to the noise floor) that can coexist with other radio signals. It is necessary that these pulses are orthogonal and also occupy an optimal amount of the frequency spectrum as allowed by the FCC mask. To this end, many pulses have been investigated by researchers. There are different pulse shapes available, but, in conventional UWB systems, Gaussian monocycles [17], Hermite polynomials [16], and prolate spheroidal wave functions [15] are very popular. However, it has been observed that these pulses have several disadvantages; for example, frequency shifting and additional filtering may be necessary to comply with the FCC spectral mask. Moreover, none of these pulses have an energy spectral density (ESD) that optimally occupies the bands defined by the FCC mask (a suboptimal ESD results in lower spectral utilization efficiency). The researchers in [12] and [13] used the sinc function to design the UWB pulses. It has been shown that the sinc function provides better spectral coverage, but it introduces ripples due to truncation. The other problem is that we cannot generate orthogonal UWB pulses for M-ary systems with the sinc function.

In this paper, we describe the design of novel UWB pulses based on zinc and frequency-domain Walsh basis functions. With proper truncation and windowing, spectrally efficient UWB pulses can be generated without the need of additional filtering. Moreover, by controlling the windowing process, different pulse durations, that is, different data rates can be achieved, imparting a high level of flexibility in the design process. We then demonstrate the performance of the proposed pulses in different modulation techniques and compare the performance with that of Gaussian monocycle pulses. We consider only the single user scenario in this paper. Multiple users and resulting inter-user interference are not considered in this work.

The rest of this paper is organized as follows. In section II, we describe the zinc and frequency-domain Walsh basis functions and their features that are employed in this study. In section III, we describe the characteristics of the spectral mask and define different translated versions of the zinc and frequency-domain Walsh basis functions that can be used to design UWB pulses yielding ESDs conforming to this mask. Section IV elaborates upon the simulation results (performed using MATLAB), including features of the proposed pulses and their comparison with other pulses in terms of spectral efficiency, time duration, autocorrelation, and crosscorrelation. Section V presents the performance analysis of the designed pulses under different modulation techniques at additive white Gaussian noise (AWGN) and multipath fading environments. Section VI concludes this paper with our observations and comments.

II. Pulse Generation

In this section, the zinc and frequency-domain Walsh basis functions are reviewed. They are thereafter employed to generate different orthogonal UWB pulses.

1. Zinc Basis Functions

The zinc basis functions are defined as linear combinations of the time-shifted versions of mutually orthogonal sinc and cosc functions:

$$z_n(t)=A_n\,\text{sinc}\left(\frac{t}{\pi}-2n\right)+B_n\,\text{cosc}\left(\frac{t}{\pi}-2n\right), \quad (2)$$

where $\text{sinc}(x)=\sin(\pi x)/(\pi x)$ and $\text{cosc}(x)=(1-\cos(\pi x))/(\pi x)$; further, A_n and B_n are constants that satisfy $A_n^2+B_n^2=1$, and n is the order of the zinc function [5]. The ESD of (2) can be expressed as a unit rectangular function with a bandwidth of 1 rad/s. That is,

$$S(\omega)=\begin{cases}1, & -1\le \omega\le 1,\\ 0, & \text{elsewhere.}\end{cases} \quad (3)$$

We can obtain infinite sets of mutually orthogonal time-shifted zinc functions with ESDs similar to (3) for different values of n [5]. For example, when $A_n=0$ and $B_n=1$, we have $z_{c,n}(t)=\text{cosc}((t/\pi)-2n)$; further, for $A_n=1$ and $B_n=0$, we have $z_{s,n}(t)=\text{sinc}((t/\pi)-2n)$. To obtain a rectangular ESD with an arbitrary bandwidth of ω_c, the above relationships can be revised as follows:

$$z_{c,n}(\omega_c t)=\text{cosc}\left(\frac{\omega_c t}{\pi}-2n\right), \quad (4)$$

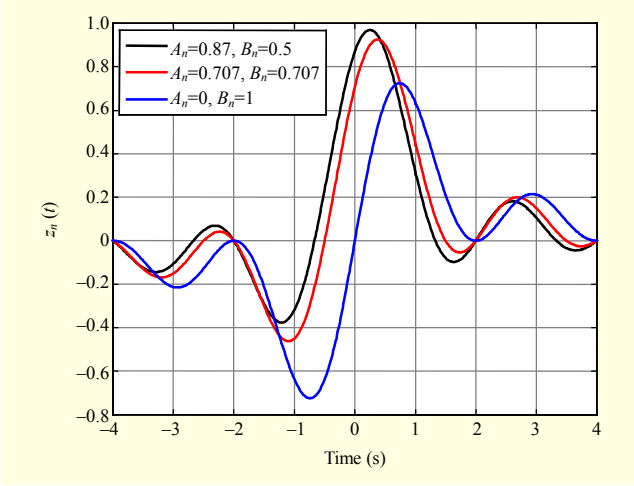

Fig. 1. Zinc basis functions for $\omega_c=2\pi$ rad/sec.

$$z_{s,n}(\omega_c t)=\operatorname{sinc}\left(\frac{\omega_c t}{\pi}-2n\right), \tag{5}$$

where $T_c=1/f_c=2\pi/\omega_c$ (f_c is the signal bandwidth in Hz). Figure 1 illustrates the first function of three zinc basis function sets. A combination of these functions will be used to generate pulses satisfying the simplified FCC mask (1).

2. Frequency-Domain Walsh Basis Functions

Walsh orthogonal signal set comprises compactly supported functions with rectangular-shaped magnitudes. Figure 2 shows the first four Walsh functions. If we consider the Walsh functions in the frequency domain, then their inverse Fourier transforms will construct an orthogonal basis for the band-limited functions. The inverse Fourier transform of the frequency-domain Walsh basis functions can be shown by

$$x_m(t)\Leftrightarrow X_m(\omega),$$

$$x_m(t)=\frac{\omega_c(-1)^{g_0}}{\pi}\left[\prod_{n=0}^{M-1}\cos\left(\frac{\omega_c t}{2^{n+1}}-g_n\frac{\pi}{2}\right)\right]\operatorname{sinc}\left(\frac{\omega_c t}{\pi 2^M}\right),$$

$$X_m(\omega)=(j)^{\alpha}(-1)^m W_m(\omega), \tag{6}$$

where $W_m(\omega)$ is the Walsh function of order m, M is the number of bits representing m, $G=\overline{g_{M-1}g_{M-2}\cdots g_1 g_0}$ is the Gray code of m, g_n is the n-th bit of G, and α is the number of Gray code bits of value one in G [14]. Figure 3 illustrates the first four frequency-domain Walsh functions for $\omega_c=2\pi\times1{,}000$ rad/s. Obviously, $|X_m(\omega)|^2=S(\omega)$, regardless of the order of the Walsh function. This feature will guarantee the band-limited nature of the signals, and it will be utilized to generate orthogonal UWB pulses satisfying the simplified FCC mask (1).

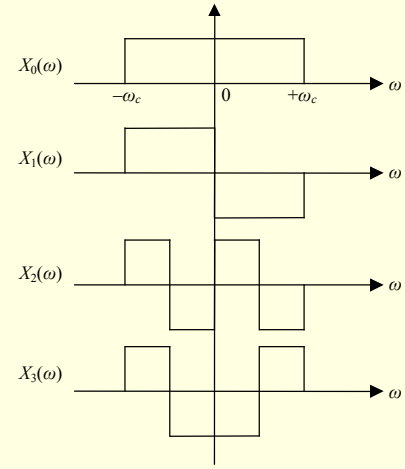

Fig. 2. First four Walsh functions.

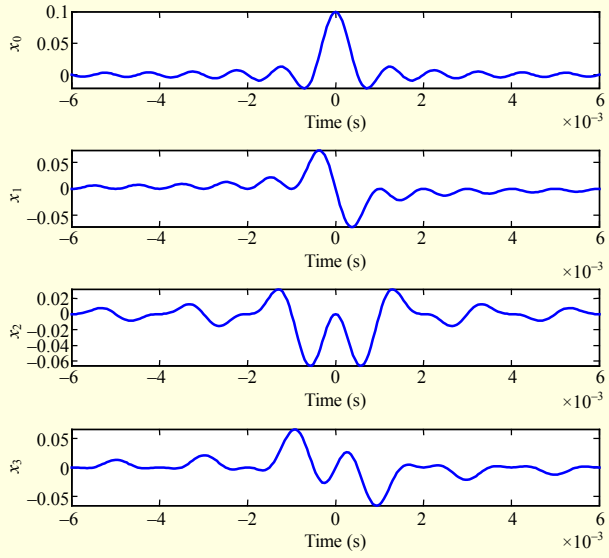

Fig. 3. Inverse Fourier transforms of first four Walsh functions ($x_m(t)$) for $\omega_c=2\pi\times1{,}000$ rad/s.

III. Generation of UWB Pulses

Now, we use the introduced band-limited functions to generate pulses whose power spectral densities are the same as the simplified version of the FCC mask (1). A closer look at (3) reveals that the simplified FCC mask (1) can be divided into three regions, that is, $R_1(\omega)$, $R_2(\omega)$, and $R_3(\omega)$, as shown in Fig. 4. This method was first used in [13]. Obviously, $R_2(\omega)$ and $R_3(\omega)$ are the modulated versions of $R_1(\omega)$ with different magnitudes. Therefore, we can express the different regions of Fig. 4 as follows:

$$|R_1(\omega)|^2=A_1^2 S\left(\frac{\omega}{\omega_{c1}}\right)=A_1^2 S\left(\frac{2\omega}{\Delta\omega_1}\right), \tag{7}$$

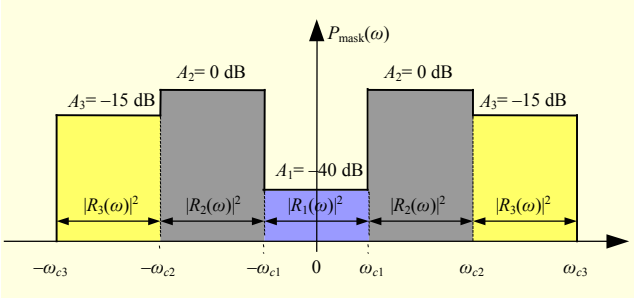

Fig. 4. Division of $P_{mask}(\omega)$ into three different regions.

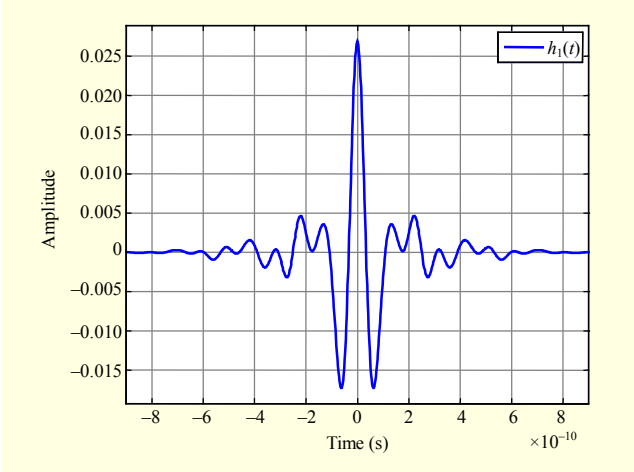

Fig. 5. UWB pulse generated based on first frequency-domain Walsh function.

$$|R_2(\omega)|^2 = A_2^2 S\left(\frac{2(\omega-\omega_{s2})}{\Delta\omega_2}\right) + A_2^2 S\left(\frac{2(\omega+\omega_{s2})}{\Delta\omega_2}\right), \quad (8)$$

$$|R_3(\omega)|^2 = A_3^2 S\left(\frac{2(\omega-\omega_{s3})}{\Delta\omega 3}\right) + A_3^2 S\left(\frac{2(\omega+\omega_{s3})}{\Delta\omega_3}\right), \quad (9)$$

where

$$\Delta\omega_1 = 2\omega_{c1} = 2\pi\times 2\times 2.1\times 10^9 \text{ rad/s},$$

$$\Delta\omega_2 = \omega_{c2} - \omega_{c1} = 2\pi\times 7.72\times 10^9 \text{ rad/s},$$

$$\omega_{s2} = (\omega_{c1} + \omega_{c2})/2 = 2\pi\times 7.05\times 10^9 \text{ rad/s},$$

$$\Delta\omega_3 = \omega_{c3} - \omega_{c2} = 2\pi\times 3.8\times 10^9 \text{ rad/s}.$$

It should be noted that the bandwidths and center frequencies of each segment in Fig. 4 are carefully determined to compensate for the sidelobes generated by truncating the time domain pulses. To prevent large sidelobes that could violate the simplified FCC mask, we can use the Kaiser window when truncating the signals. This will result in a larger transition region, but this is an acceptable tradeoff.

To obtain the UWB pulses, we can use either zinc or frequency-domain Walsh basis functions to generate the segments of the signal whose ESD is shown in Fig. 4. These pulses can be expressed as

$$\begin{aligned} r_n(t) = {} & A_1 \cdot \frac{\Delta\omega_1}{2\pi} \cdot s_n\left(\frac{\Delta\omega_1 t}{2}\right) \\ & + 2A_2 \cdot \frac{\Delta\omega_2}{2\pi} \cdot s_n\left(\frac{\Delta\omega_2 t}{2}\right) \cdot \cos(\omega_{s2}\, t) \\ & + 2A_3 \cdot \frac{\Delta\omega_3}{2\pi} \cdot s_n\left(\frac{\Delta\omega_3 t}{2}\right) \cdot \cos(\omega_{s3}\, t). \end{aligned} \quad (10)$$

where $s_n(t)$ denotes any zinc or frequency-domain Walsh basis function. Figures 5 and 6 illustrate the generated UWB pulses using the first and second frequency-domain Walsh functions, respectively. Here, we use $h_n(t)$ and $q_n(t)$ to denote the n-th UWB Walsh-based and zinc-based functions, respectively.

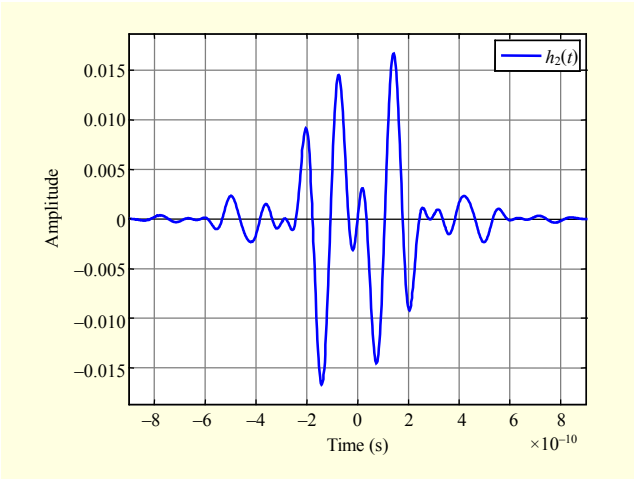

Fig. 6. UWB pulse generated based on second frequency-domain Walsh function.

IV. Simulation Results

1. Pulse Duration

Theoretically, transmitting ideal band-limited pulses, whose lengths are infinite, is not feasible, though they are the best fit for the UWB spectral mask. Consequently, in real systems, such pulses need to be truncated to make the lengths finite. However, truncating the pulse introduces sidelobes in the ESD, due to the Gibbs phenomenon. After truncation, spectral changes in the pulse play a vital role in deciding the length of the pulse and the truncation technique to be employed. The longer the time duration of a pulse, the more spectrally efficient it is [7]. However, if the pulse duration increases, it results in an overall sluggish wireless system response. Thus, there is a tradeoff between the length of the pulse, its spectral behavior, and the bitrate of the targeted communication system.

To mitigate this, a non-rectangular window, such as the Kaiser window, is used to uniquely control the tradeoff between the main-lobe width and sidelobe area. The simulation results performed in this study reveal that even after truncation and windowing, we can obtain almost orthogonal finite-length pulses that satisfy the constraints of the FCC mask by slightly modifying ω_{c1}, ω_{c2}, ω_{c3}, A_1, A_2, and A_3.

2. Spectral Efficiency

The spectral utilization efficiency of the designed pulses can be measured in terms of the normalized effective signal energy (NESE), defined as

$$\beta = \frac{\int P_h(f)\mathrm{d}f}{\int P_{\mathrm{mask}}(f)\mathrm{d}f}, \tag{11}$$

where $P_h(f) = |H(f)|^2$, $H(f)$ is the Fourier transform of the transmitted pulse and $P_{\mathrm{mask}}(f)$ is the ESD of the mask (1) [6].

To obtain pulses that efficiently utilize the allowed spectrum, β should be as close to 1 as possible. Since the data rate is inversely proportional to the pulse duration T, an ideal pulse for communication signaling should have large β and small T. This situation is difficult to achieve due to the uncertainty principle of the Fourier transform.

With the proposed zinc-based and Walsh-based pulses, we are able to achieve a spectral efficiency between 0.75 and 0.95. From Fig. 7, it can be seen that the spectral efficiency of the first pulses based on Walsh ($h_1(t)$) and zinc ($q_1(t)$) are 0.89 and 0.92, respectively.

3. Autocorrelation and Crosscorrelation

In wireless communication and signal processing applications, autocorrelation and crosscorrelation functions have great significance, as they determine the bit error rate (BER) performance of the system [8]. There are certain differences between autocorrelation and crosscorrelation functions. First, the autocorrelation function measures the degree of similarity of the signal with the time-shifted version of itself.

However, crosscorrelation measures the degree of similarity between two different signals when one of them is shifted in time. Second, while the autocorrelation coefficient for the zero time delay must be 1, the crosscorrelation coefficient for the zero time delay can take on any value between –1 and 1. Third, the peak of the crosscorrelation of two signals may not occur at the zero time delay. However, the peak of the autocorrelation of a signal must always occur at the zero time delay (assuming the signal is not periodic). Fourth, unlike the autocorrelation function, the crosscorrelation function may not be symmetric.

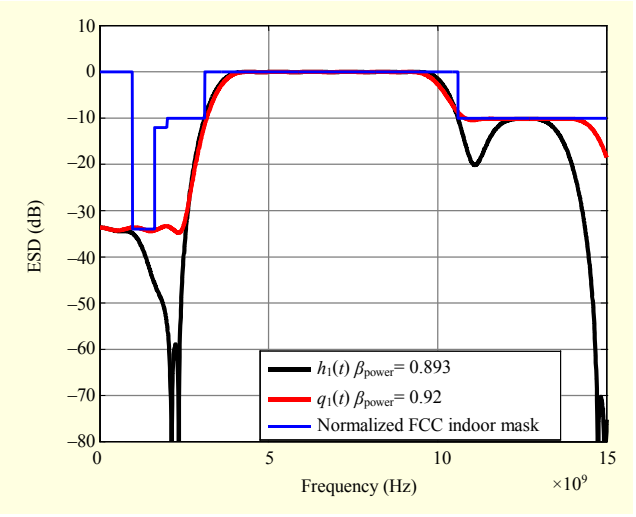

Fig. 7. ESD of signals $h_1(t)$ and $q_1(t)$ with normalized FCC indoor mask given as reference.

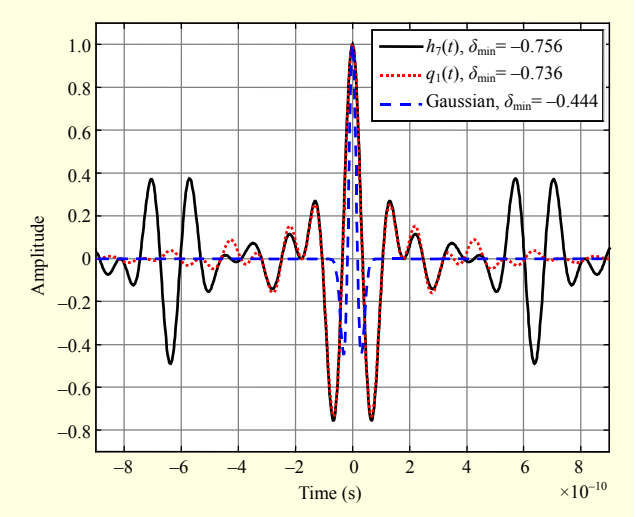

Fig. 8. Autocorrelation of $q_1(t)$, $h_7(t)$, and 2nd Gaussian monocycle.

Autocorrelation is more useful in pulse position modulation (PPM) in which a single pulse is used and information is conveyed by the timings of the transmission relative to a reference instant. In our simulation, we use the zinc-based pulse $q_n(t)$ and the Walsh-based pulse $h_n(t)$ and their respective delayed version, $q_n(t–\delta)$ and $h_n(t–\delta)$, to represent binary data (0 or 1). The optimum value for the delay δ is the time when the autocorrelation function takes its minimum value. Such a choice for δ minimizes the probability of a bit error (as discussed in a later section).

Figure 8 illustrates the autocorrelation plot of the finite-length discrete-time Walsh-based and zinc-based pulses. The minimum of the autocorrelation function determines the modulation performance. As clearly shown in Fig. 8, the

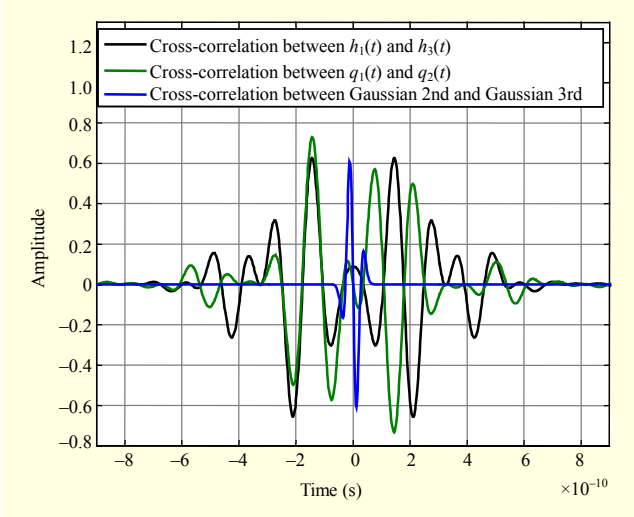

Fig. 9. Crosscorrelation of zinc-based, Walsh-based, and Gaussian monocycle UWB pulses.

Walsh-based and zinc-based pulses have better minimum value of autocorrelation than the 2nd Gaussian monocycle has, which results in a better BER performance in PPM modulation. Also, another interesting parameter is the time shift δ, at which time the minimum autocorrelation occurs. The maximum number of pulses that can be transmitted per second with PPM is $(T+\delta)^{-1}$. If the time shift is smaller, more signals can be transmitted per unit time, resulting in a higher data throughput. From the figure, it is apparent that the 2nd Gaussian monocycle has smaller time shift between pulses for the price of a smaller autocorrelation minimum, which results in a worse BER performance.

Figure 9 illustrates the crosscorrelation plot of the zinc-based, Walsh-based, and Gaussian monocycle UWB pulses. It should be noted that if the crosscorrelation of the signals is small for a comparatively long period around zero or it has a slow varying zero crossing, then the designed pulses are robust against timing jitter when both signals are used for modulation (such as pulse shape modulation). Considering this fact, the Walsh-based and zinc-based pulses have more robust timing jitter performances than the Gaussian monocycle pulses have. This is confirmed with the pulses' performances in the multipath fading environment.

V. Bit Error Rate Performance

The performances of the generated pulses are evaluated under different modulation schemes, namely, binary PPM (2-PPM), binary pulse shape modulation (2-PSM), and quaternary PSM (4-PSM). In this section, we elaborate upon the BER for each modulation scheme as a function of the modulation order and the signal-to-noise ratio (SNR).

1. Gaussian Noise Channels

In PPM, information is conveyed by the position of the pulse (presence or absence of a time shift) in the frame. The optimum value of the time shift δ_{optimum} is the instant when the most negative correlation value between the reference pulse and its time-shifted version is obtained [9]. The theoretical BER (P_B) of generic non-orthogonal signals with minimum autocorrelation value r in the presence of AWGN can be expressed as

$$P_B = Q\left(\sqrt{(1-r)\frac{E_b}{N_0}}\right), \tag{12}$$

where E_b is the average bit energy, N_0 is the one-sided Gaussian noise power spectral density, and $Q(\cdot)$ denotes the co-error function. Since the $Q(\cdot)$ function is a decreasing function of its argument, a better minimum value of the autocorrelation function results in a better BER performance.

The PSM technique is a modulation scheme that employs different (typically orthogonal) waveforms to convey information. For M-ary orthogonal signaling, we can upper bound the BER as (from [7])

$$P_B < \left(\frac{M}{2(M-1)}\right) Q\left(\sqrt{\frac{(E_b.\log_2 M}{N_0}}\right). \tag{13}$$

In our simulation, we use binary PSM, namely, 2-PSM (M=2), and quaternary PSM, namely 4-PSM (M=4). The BER functions for these two schemes can be respectively obtained from (13) as

$$P_B = Q\left(\sqrt{\frac{E_b}{N_0}}\right) \tag{14}$$

and

$$P_B < \frac{2}{3} Q\left(\sqrt{\frac{2E_b}{N_0}}\right). \tag{15}$$

Note that (14) is an exact formula for the BER, but (15) is only an upper bound that is tight at moderate to high SNRs. Figure 10 shows the BER curves for the above-mentioned modulation schemes under an AWGN channel environment when the proposed pulses are used. Performances of the Gaussian monocycles are also shown for comparison. The Walsh-based and zinc-based pulses employed for each modulation scheme are given in the legends of Fig. 10. For the 2-PPM case, the BER performance of our pulses is comparable to that of the signals described in [9]; however, the NESE values of our pulses are higher. A higher NESE value allows for transmitting the pulse at a higher energy level while conforming to the same ESD, thereby increasing the communication range and/or fidelity.

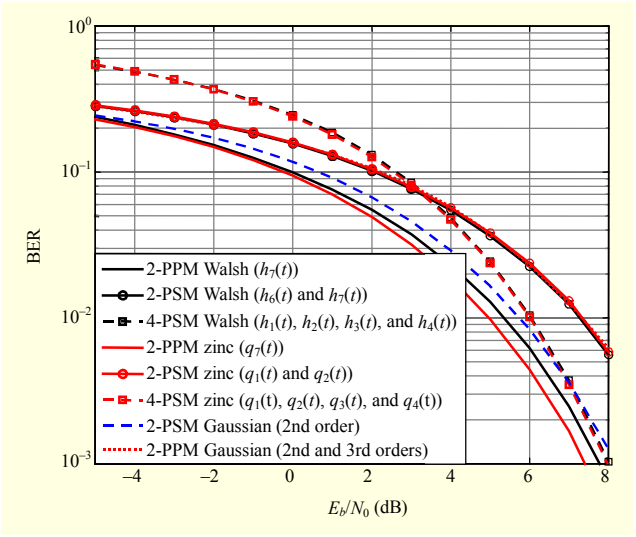

Fig. 10. BER performance under AWGN.

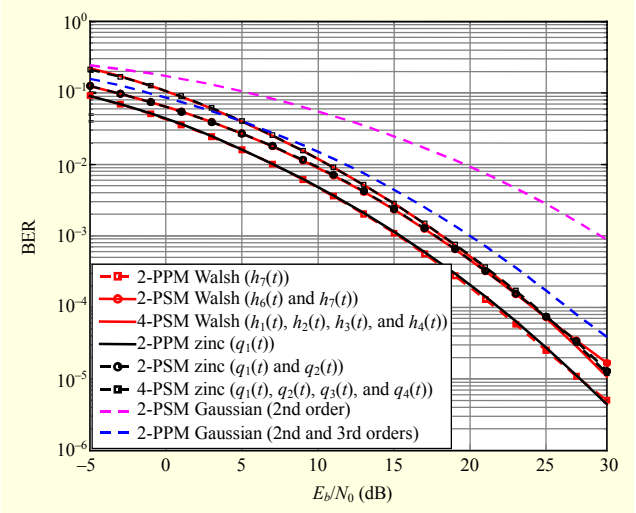

Fig. 11. BER performance under Multipath fading environment.

With the orthogonal PSM, the performances of all pulses are similar. Using the design technique described in this paper, we can generate an arbitrary number of orthogonal pulses for use in the PSM modulations. For higher orders of PSM modulation, the BER improves; however, the receiver complexity increases exponentially—this is a tradeoff that is an important aspect of communication system design. From the BER curves for the 4-PSM technique, it can be seen that even after truncation and windowing (which may affect the orthogonality of the signals), a desirable level of BER performance can be achieved with the proposed Walsh-based and zinc-based pulses. Lastly, as we expected, 4-PSM outperforms 2-PSM at a moderate to high SNR. Since multiple orthogonal signals cannot be obtained with Gaussian monocycle pulses, they cannot be used in PSM communication systems.

2. Multipath Fading Channels

The received signal in a wireless communication system is typically an attenuated, delayed, and distorted version of the transmitted signal, in addition to being corrupted by noise and interference. In most propagation environments, the signal arriving at the receiver is a combination of multiple reflected paths. This phenomenon is called multipath propagation. In this kind of complex physical environments, accurate knowledge of the channel through which the signals will traverse is important to design and evaluate wireless systems [3]. Different channel models have been developed for different environments.

Three channel models are usually considered for multipath analysis: the Rayleigh tapped-delay-line model, Saleh-Valenzuela (S-V) model, and Δ−*K* model. It has been shown that the S-V model is best suited to the measured channel characteristics, such as the mean excess delay, mean RMS delay spread, and mean number of significant paths within 10 dB of the peak multipath arrival [11]. The S-V model uses a log-normal distribution for the average power in the received multipath components. Each path gain is further modeled as a Rayleigh distributed random variable. Also, an independent fading mechanism is considered for each cluster and for each ray within a cluster. In the S-V model, both the cluster and ray arrival times are modeled independently by Poisson-distributed random variables. These advantages have made the S-V model very popular to formulate the multipath propagation characteristics of the wireless channel.

Based on the presence of clusters in most UWB measurement environments reported in the literature, a modified version is proposed on the basis of the conventional S-V channel model [11]. This modified version accounts for the clustering of multipath components and can be represented as follows [11]:

$$g(t) = \sum_{l=0}^{L} \sum_{k=0}^{K_l} a_{k,l}\,\delta(t - T_l - \tau_{k,l}), \qquad (16)$$

where $1+L$ is the number of clusters, $1+K_l$ is the number of multipath components within the l-th cluster, and $a_{k,l}$ is the multipath gain coefficient of the k-th component in the l-th cluster. Here, T_l is defined as the time of arrival of the first arriving multipath component within the l-th cluster and can be called the delay of the l-th cluster. Further, $\tau_{k,l}$ is the delay of the k-th multipath component relative to the arrival time of the l-th cluster, T_l. The clustering channel model relies on two classes of parameters, namely, inter-cluster and intra-cluster parameters, which characterize the cluster and multipath component, respectively. From (16), $\{L, T_l\}$ and $\{K_l, \tau_{k,l}, a_{k,l}\}$ are classified as the inter-cluster and intra-cluster parameters, respectively.

Figure 11 shows a comparison of the BER performances for different modulation schemes on multipath channels. The multipath channel used in this simulation is generated with the S-V model using parameters L=1 and K_f=9. The graphs show that the Walsh-based and zinc-based pulses have much better BER performances than the Gaussian monocycles have when PPM is employed for communication. This can be attributed to the overall better crosscorrelation and autocorrelation properties of these pulses compared to the Gaussian monocycle pulses. Both Walsh-based and zinc-based pulses exhibit desirable performance when employed in orthogonal PSM (2-PSM and 4-PSM) modulation schemes. The Gaussian monocycles exhibit significant BER degradation when employed in 2-PSM, due to their suboptimal crosscorrelation properties. These simulation results show that the proposed zinc-based and Walsh-based pulses exhibit excellent BER properties when employed on fading channels.

VI. Conclusion

In this study, we successfully designed a set of UWB pulses based on the frequency-domain Walsh and zinc basis functions. The ESDs of these pulses conformed to the emission levels defined by the FCC mask. Theoretically, by using the formulated closed-form expressions, an infinite number of zinc-based and Walsh-based orthogonal pulses can be generated. Moreover, the truncated and windowed versions of these pulses exhibited very high NESE values for reasonably short time durations. Finally, the designed pulses were evaluated for use in PPM and PSM communication techniques, and our simulations showed that these pulses result in better BER performances than those obtained by the Gaussian monocycles. An extension of the proposed ideas to a multiuser scenario and analysis of the resulting multiuser interference are topics for future work.

References

[1] "Giga Bits per Second Wireless at 60 GHz: Ultra Wide Band and Beyond," Executive Technology Report, Peter Andrews interviews Brian Gaucher, Sunday, Mar. 28, 2010. Website: http://users.ece.utexas.edu/~wireless/General/60ghz/systems01.pdf

[2] FCC Report and Order, *In the Matter of Revision of Part 15 of the Commission's Rules Regarding Ultrawideband Transmission Systems*, FCC 02-48, Apr. 2002.

[3] M. Ghavami, L.B. Michael, and R. Kohno, *Ultra Wideband Signals and Systems in Communication Engineering*, Sussex, England: Wiley, 2007.

[4] X. Wu et al., "Optimal Waveform Design for UWB Radios," *IEEE Trans. Signal Process.*, vol. 54, no. 6, June 2006, pp. 2009-2021.

[5] R.A. Sukkar, J.L. LoCicero, and J.W. Picone, "Decomposition of the LPC Excitation Using the Zinc Based Functions," *IEEE Trans. Acoustics, Speech, and Signal Process.*, vol. 37, no. 9, Sept. 1989, pp. 1329-1340.

[6] M. Mandal and A. Asif, *Continuous and Discrete Time Signals and Systems*, UK: Cambridge University Press, 2007.

[7] B. Sklar, *Digital Communications: Fundamentals and Applications*, 2nd ed., Upper Saddle River, NJ: Prentice-Hall, Inc., 2001.

[8] J.G. Proakis and M. Salehi, *Digital Communications*, 5th ed., McGraw-Hill Science/Engineering/Math, 2007.

[9] J.A. da Silva and M.L.R. de Campos, "Spectrally Efficient UWB Pulse Shaping with Application in Orthogonal PSM," *IEEE Trans. Commun.*, vol. 55, no. 2, Feb. 2007, pp. 313-321.

[10] Q. Spencer et al., "A Statistical Model for Angle of Arrival in Indoor Multipath Propagation," *IEEE Veh. Technol. Conf.*, vol. 47, 1997, pp. 1415-1419.

[11] A. Saleh and R. Valenzuela, "A Statistical Model for Indoor Multipath Propagation," *IEEE J. Sel. Areas Commun.*, vol. 5, no. 2, Feb. 1987, pp. 128-137.

[12] N.C. Beaulieu and B. Hu, "A Pulse Design Paradigm for Ultra-Wideband Communication Systems," *IEEE Trans. Wireless Commun.*, vol. 5, no. 6, June 2008, pp. 1274-1278.

[13] N.C. Beaulieu and B. Hu, "On Determining a Best Pulse Shape for Multiple Access Ultra-Wideband Communication Systems," *IEEE Trans. Wireless Commun.*, vol. 7, no. 9, Sept. 2008, pp. 3589-3596.

[14] K.H. Siemens and R. Kita, "A Nonrecursive Equation for the Fourier Transform of a Walsh Function," *IEEE Trans. Electromagn. Compat.*, vol. EMC-15, no. 2, May 1973, pp. 81-83.

[15] R.S. Dilmaghani et al., "Novel UWB Pulse Shaping Using Prolate Spheroidal Wave Functions," *Proc. PIMRC*, 2003.

[16] L.B. Michael, M. Ghavami, and R. Kohno, "Multiple Pulse Generator for Ultra-wideband Communication Using Hermite Polynomial Based Orthogonal Pulses," *Proc. IEEE Conf. Ultra Wideband Systems and Technologies*, 2002, pp. 47-51.

[17] B. Allen, S.A. Ghorashi, and M. Ghavami, "A Review of Pulse Design for Impulse Radio," *IEE Seminar Ultra Wideband Commun. Technol. System Design*, 2004, pp. 93-97.

Praveen Chaurasiya received his BSc (Eng) in electrical engineering from SGSITS, Indore, India, in 2005. He received his MSc in electrical engineering from San Diego State University, San Diego, CA, USA, in 2010, where he was appointed as the research assistant for the topic "Haar-based Orthogonal Signals for Ultra Wide Band Pulse Generation: Design and Performance Analyses." Currently, he works as an RF engineer for Qualcomm Incorporated.

Ashkan Ashrafi received his BSc and MSc in electronics engineering from K.N.Toosi University of Technology, Tehran, Iran, and MSE and PhD in electrical engineering from the University of Alabama in Huntsville, Huntsville, AL, USA, in 1991, 1995, 2003, and 2006, respectively (all with the highest honor). He served as a visiting assistant professor in the Electrical and Computer Engineering Department of the University of Alabama in Huntsville from 2006 to 2007. He is currently an assistant professor in and director of the Real-Time DSP and FPGA Development Laboratory in the Electrical and Computer Engineering Department and an adjunct professor in the Computational Science Research Center at San Diego State University, San Diego, CA, USA. He received the Outstanding Faculty Award of the Department of Electrical and Computer Engineering, San Diego State University, in 2012. He received the 2005 Iliana Martin Chittur Outstanding Graduate Student Award and the 2005 National Engineer's Week Outstanding Graduate Student Award from the College of Engineering, University of Alabama in Huntsville. His research interests are digital and statistical signal processing, direct digital frequency synthesizers, and applied mathematics.

Santosh Nagaraj received his BTech in electrical engineering from the Indian Institute of Technology, Madras, India, in 2000 and his PhD from Purdue University, West Lafayette, IN, USA, in 2005. Since 2005, he has been a member of the faculty of San Diego State University, San Diego, CA, USA, where he is currently an associate professor of electrical and computer engineering. His research interests are primarily in the areas of communication system design, broadband modulation and demodulation techniques, and signal processing. He is currently working on adaptive modulation and coding for orthogonal frequency division multiplexing systems with feedback and on the design of efficient coding techniques for block fading channels. His other research interests include multiple antenna systems and power control. He has served as a reviewer for several prestigious journals and professional conferences. He has also served on the technical program committee for the IEEE Wireless Telecommunications Symposium.